DOI: 10.15587/978-617-7319-97-8.CH1

Orest Ostash, Svitlana Polyvoda, Andrii Titov,
Kostyantyn Balushok, Roman Chepil, Natalia Zlochevska

CHAPTER 1

CAST AND DEFORMATION STRENGTHENED ALLOYS OF THE Al-Mg-Sc SYSTEM

ABSTRACT

The effect of reducing the magnesium content and doping with scandium, zirconium, manganese, chromium, and rare-earth metals on the structure, phase composition, strength, plasticity, and crack resistance, as well as the potential and corrosion current of alloys of the Al-Mg and Al-Mg-Sc systems obtained using magnetohydrodynamic foundry was investigated. Installation a positive effect of reducing the magnesium content, replacing manganese with chromium, and alloying with lanthanum in alloys of the Al-Mg-Sc system in the cast state and after deformation processing (extrusion, pressing, and rolling) was established. It is shown that due to dispersion strengthening by secondary intermetallics of chromium and lanthanum, this alloy in the cast state after homogenization is superior in strength to the well-known alloys of grades 1570 and 1545. After hot and cold rolling, it is not inferior to these alloys in terms of strength and plasticity, but has higher corrosion resistance characteristics. It was found that in terms of structural strength, which is comprehensively determined by the characteristics of strength and cyclic crack resistance, such alloys are superior to the well-known Al-Mg-Sc, Al-Mg and Al-Cu-Mg systems. The results of modeling the stress-strain state and damage of strips of different thicknesses during hot isothermal pressing are presented. The temperature-force parameters of the process and the geometry of the pressed strip are set to obtain its minimal damage.

KEYWORDS

Aluminum alloys, Al-Mg-Sc system, alloying, chrome, REM, deformation treatment, structure, structural strength, corrosion resistance, damage.

The high characteristics of plasticity, corrosion resistance and weldability, as well as the absence of the need to perform strengthening heat treatment, determine the wide use of alloys of the Al-Mg system (AMg type) in mechanical engineering, in particular in aerospace engineering. But their disadvantage is low strength [1], which is increased by structural (shredding structural elements) and solid-solution or intermetallic strengthening, in particular, alloying with transition metals, among which scandium is one of the most effective [2, 3]. Doping with scandium ensures the formation of a dendritic structure of castings with small crystals of solid aluminum solution in the form of cells and dispersed intermetallic inclusions. At the same time, in order to increase the corrosion resistance and weldability and manufacturability in a high-strength state, it is considered appropriate to reduce the magnesium content from 6.0...6.5 to 4.0...4.5 by wt. % [3, 4].

1.1 STRUCTURE AND MECHANICAL AND CORROSION PROPERTIES OF CAST ALLOYS OF THE Al-Mg-Sc SYSTEM

The properties of cast alloys depend significantly on the casting technology: homogenization of the melt, speed of crystallization, etc. Today, one of the progressive technologies is the technology based on the use of magnetohydrodynamic (MHD) foundry installations. Here, the simultaneously controlled thermal and force effects on the liquid metal contribute to the rapid and complete assimilation of alloying and modifying elements, the uniformity of the chemical composition and the grinding of the structure, as well as the intensification of vacuum refining [5, 6].

The structure and properties of alloys of the Al-Mg and Al-Mg-Sc systems [7] were studied, in particular the well-known AMg_6 (option No. 1) and 1570 and 1545 with different Mg contents (options No. 2, 3), as well as experimental alloys with different contents Zr, Mn and Cr (options No. 4–8 in **Table 1.1**). Samples were cut from castings obtained by MHD mixing of the melt at 700±10 °C. To homogenize the structure of the casting during the decomposition of the solid solution, the alloys were crystallized in a steel mold heated to 300 °C.

Table 1.1 Chemical composition (wt. %) of the investigated alloys

Alloy No.	Mg	Mn	Sc	Zr	Cr	Fe	Si
1	6.28	0.39	–	–	–	0.12	0.18
2	5.96	0.40	0.24	0.09	–	0.28	0.16
3	4.61	0.43	0.28	0.12	–	0.31	0.17
4	4.50	–	–	0.49	–	0.23	0.17
5	4.47	–	–	0.75	–	0.14	0.16
6	4.53	0.42	–	0.25	–	0.21	0.18
7	4.70	–	–	0.30	0.43	0.10	0.09
8	4.60	–	0.26	0.13	0.47	0.14	0.10

Note: the averaged chemical composition is given; all alloys also contain ~0.03 wt. % Ti and ~0.003 wt. % Be, Al – the rest

AMg_6 alloy (option No. 1) has low strength and plasticity (**Table 1.2**), which is characteristic of this type of cast alloys, when a non-dendritic cellular matrix structure with a large grain size (up to 100...200 μm) and a network of large (micro-sized) discharges is formed secondary phase up to 20...40 μm in size (**Fig. 1.1, *a*, *b***). Based on the results of local chemical analysis (**Table 1.3**), it can be stated that the matrix is a solid solution of Mg, Mn, and Ti in aluminum, and the secondary phase is intermetallics such as Al_3Mg_2, Al_8Mg_5, Al_6(Fe, Mn), Mg_2Si [8].

Table 1.2 Mechanical characteristics of alloys

Characteristics	Alloy No.							
	1	**2**	**3**	**4**	**5**	**6**	**7**	**8**
$\sigma_{0.2}$, MPa	137	152	178	90	91	93	109	175
σ_B, MPa	213	234	284	214	204	205	244	280
Δ_5, %	8	11	14	16	11	15	18	15

Note: alloy number according to **Table 1.1***; averaged test data of 3–5 samples are presented*

Scandium and zirconium in alloy type 1570 (option No. 2) increase its mechanical characteristics compared to option No. 1 (**Table 1.2**) primarily due to grinding of the matrix grain (**Fig. 1.1, *c*** vs. **Fig. 1.1, *a***). The morphology of large intermetallics did not change significantly (**Fig. 1.1, *d*** vs. **Fig. 1.1, *b***). At the same time, as evidenced by the data in the **Table 1.3**, a dispersed (nano-sized) Al_3Sc strengthening phase is formed in the matrix [2, 3], but zirconium (together with scandium) is contained only in large intermetallics. A high iron content was recorded here (**Table 1.3**). Obviously, in addition to Al_6(Fe, Mn)-type precipitates, Al_3Fe-type intermetallics are formed [8]. Iron-based intermetallics negatively affect the properties of Al-Mg-Sc alloys [8, 9], so it is suggested to limit the content of iron and silicon in them: $[Fe+Si] \leq 0.12$ wt. %.

An unexpected result was obtained by studying an alloy of type 1545 with a reduced magnesium content (option No. 3 in **Table 1.1**). It is known that the strength of alloys of the Al-Mg system increases with increasing magnesium content. Option No. 3 shows the opposite trend (**Table 1.2**), when with a decrease in magnesium content from 5.96 to 4.61 wt. %, but with a slightly higher content of scandium and zirconium (**Table 1.1**), the strength and plasticity of the alloy increased significantly. There was a transformation of the morphology of the structure of large discharges of the secondary phase (**Fig. 1.1, *e*, *f*** vs. **Fig. 1.1, *c*, *d***), in particular, their size decreased and their distribution became more uniform. However, the nature of the matrix changed the most (**Table 1.3**): zirconium appeared here, which indicates the formation of a dispersed $Al_3(Sc_{1-x}Zr_x)$ phase at an optimal ratio of $Sc/Zr \approx 2/1$. This phase determines the grinding of the grain, provides a more homogeneous non-dendritic structure and strengthening of the alloy, which, in our opinion, is also facilitated by the used MHD technology.

Increasing the amount of zirconium (0.25...0.75 wt. %) in alloys with a reduced magnesium content without and with manganese (options No. 4–6 in **Table 1.1**) did not have a positive effect on improving their mechanical characteristics compared to option No. 1 (**Table 1.2**).

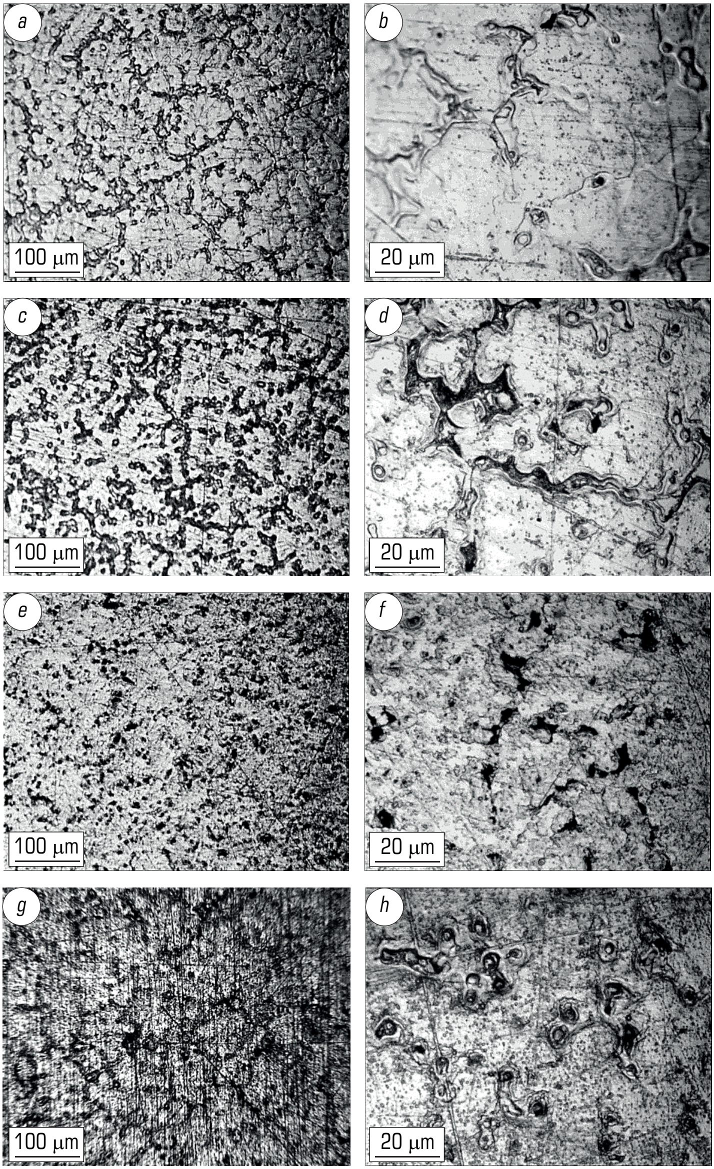

Fig. 1.1 Microstructure of alloys: *a*, *b* – No. 1; *c*, *d* – 2; *e*, *f* – 3; *g*, *h* – 8

Table 1.3 Local content (wt. %) of chemical elements in the investigated alloys

Structural component		Chemical element	Alloy No. 1	2	3	8
Matrix		Al	94.34	95.31	96.26	96.20
		Mg	5.23	4.25	3.02	2.76
		Mn	0.36	0.22	0.28	–
		Sc	–	0.22	0.24	0.22
		Zr	–	–	0.11	0.12
		Cr	–	–	–	0.64
		Ti	0.04	0.05	0.05	0.04
		Fe	–	–	–	–
		Si	–	–	–	–
Micro-sized intermetallics	Zone A	Al	83.17	86.02	88.06	88.02
		Mg	15.85	13.12	10.22	10.60
		Mn	0.48	0.10	0.48	–
		Sc	–	0.13	0.32	0.38
		Zr	–	0.16	0.05	0.07
		Cr	–	–	–	0.16
		Ti	–	–	–	–
		Fe	0.32	0.45	0.63	0.36
		Si	0.16	–	0.22	0.40
	Zone B	Al	76.18	67.09	68.69	73.50
		Mg	23.44	8.60	10.12	11.40
		Mn	0.12	1.40	2.87	–
		Sc	–	0.39	0.47	0.60
		Zr	–	0.21	0.28	0.35
		Cr	–	–	–	13.72
		Ti	0.05	–	–	–
		Fe	–	22.06	17.27	0.41
		Si	0.18	0.23	0.26	–

*Note: alloy number according to table 1; averaged data of 3–5 measurements are provided; zone A is dark, and zone B is the light part of intermetallics (***Fig. 1, *b*, *d*, *f*, *h****)*

In alloys of the Al-Mg-Sc-Zr system, manganese content is 0.2...0.6 wt. % increases their strength and corrosion resistance [2, 4]. There are also known attempts to alloy such alloys with manganese (~0.5 wt. %) and chromium (~0.5 wt. %) in order to additionally form a strengthening phase of the Al_7Cr type [10]. The influence of chromium on the properties of alloys of the Al-Mg and Al-Mg-Sc system has been little studied. Although, to improve the properties of the weld metal of welded joints of these alloys, welding wires with the addition of chromium were used [2]. However, the properties of such alloys after replacing manganese with chromium were not investigated.

In alloys of the Al-Mg-Zr system, such a replacement (options No. 6, 7 in **Table 1.1**) led to a noticeable increase in the strength and plasticity of alloy No. 7 compared to option No. 6 (**Table 1.2**). Therefore, they studied alloy type 1545 (option No. 3), which contained 0.47 wt. % Cr instead of 0.43 wt. % Mn (option No. 8). For this alloy, a matrix structure with a grain size of 50...100 μm was recorded (**Fig. 1.1, *g***) with a uniform distribution of globular particles of the intermetallic phase with an average size of ~10 μm (**Fig. 1.1, *h***). Scandium, zirconium and chromium were found in the matrix (**Table 1.3**), which may indicate the formation of dispersed strengthening phases of the type $Al_3(Sc_{1-x}Zr_x)$ and Al_7Cr. These elements in large quantities (especially chromium) are present in large intermetallics, where the iron content is quite low compared to option No. 3. As a result, alloying with chromium instead of manganese ensured the strength and plasticity of alloy No. 8 at the level of alloy No. 3 (**Table 1.2**), but had a significant positive effect on its corrosion resistance.

Electrochemical studies revealed (**Fig. 1.2**) that with an increased magnesium content (6.0...6.3 wt. %) the alloy type 1570 (option No. 2) compared to the alloy type AMg_6 (option No. 1) has a slightly better corrosion potential E_{cor}, but the corrosion current I_{cor} is almost 4 times higher (**Fig. 1.2**), which causes a greater intensity of corrosion of the surface of the samples in a 3 % NaCl solution (**Fig. 1.3, *b*** vs. **Fig. 1.3, *a***). Such an increase in I_{cor} values can be associated with an increase in the heterogeneity of the structure of alloy No. 2, in particular, with the formation of large intermetallics with a high iron content (**Table 1.3**).

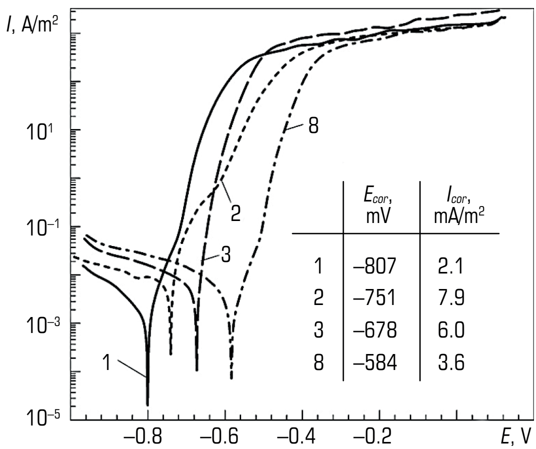

Fig. 1.2 Polarization curves and electrochemical characteristics of alloys according to their number in the **Table 1.1**

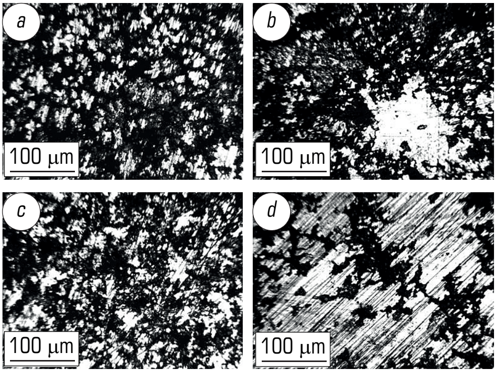

Fig. 1.3 Corroded surface of alloy samples No. 1 (*a*); No. 2 (*b*); No. 3 (*c*) and No. 8 (*d*). Alloy number according to the **Table 1.1**

With a decrease in the magnesium content, which is among the first (standard electrode potential z^*=–2.363 V) in the range of activity of metals [11], the polarization curve of alloy No. 3 shifts to the right and down, i.e., the values of E_{cor} and I_{cor} improve (**Fig. 1.2**), which is manifested in a decrease in the intensity of corrosion of the sample surface (**Fig. 1.3, *c*** vs. **Fig. 1.3, *b***). However, the optimal situation was observed for alloy No. 8: here the best combination of E_{cor} and I_{cor} characteristics was recorded (**Fig. 1.2**), and the traces of corrosion on the surface of the sample are the smallest (**Fig. 1.3, *d***), which is a consequence of the positive effect of chromium, for which z^*=–0.744…0.913 V versus –1.180 V for manganese [11].

Thus, in contrast to the known literature data, an increase in the strength limit was recorded due to a decrease in the magnesium content in alloys of the Al-Mg-Sc system, obtained using the technology of magnetohydrodynamic mixing of the melt at 700 °C and its crystallization in a steel mold heated to 300 °C. It was established that chromium effectively replaces manganese in these alloys, ensuring their strengthening and a significant increase in corrosion resistance in a 3 % NaCl solution.

1.2 STRENGTH AND CYCLIC CRACK RESISTANCE OF HEAT-DEFORMED ALLOYS OF THE Al-Mg-Sc SYSTEM

Optimum characteristics of strength and plasticity are achieved after thermo-deformation processing of cast blanks: extrusion, pressing, rolling, etc. The chemical composition and structural phase state can have different effects on the strength and crack resistance of deformed alloys of the Al-Mg-Sc system under cyclic loading, in particular on the fatigue threshold [12]. Therefore, the structural strength of materials, especially for aerospace purposes, when the principle of safe damage is applied during their operation, depends on the optimal combination of strength and crack resistance characteristics. It can be effectively estimated [13] by the complex parameter $P=[\sigma_B \cdot \Delta K_{th} \cdot \Delta K_{fc}]$, where σ_B – the limit of strength; ΔK_{th} – the fatigue threshold and ΔK_{fc} – the cyclic fracture toughness, which are characteristics of the cyclic crack resistance (CCR) of the material [14].

Alloys 1570 and 1545 with different magnesium content were studied (**Table 1.4**). Castings were obtained by MHD mixing of the melt at 700±10 °C and crystallization in a steel mold heated to 300 °C to homogenize the structure of the casting.

The resistance to plastic deformation of the metal was evaluated based on the temperature dependence of the yield strength under compression (**Fig. 1.4**), determined on standard samples cut from castings. On this basis, thermal deformation treatment was carried out in different ways: by extrusion of castings ∅ 30 mm to ∅ 20 mm at 390±10 °C (alloy No. 1) and 420±10 °C (alloy No. 2); pressing castings ∅ 30 mm into a strip 6 mm thick at 420±10 °C; by rolling pressed blanks 20 mm thick onto a plate 4.5 mm thick at 420±10 °C (alloy No. 1) and 460±10 °C (alloy No. 2) [15].

Table 1.4 Chemical composition (wt. %) of alloys

Alloy No.	Mg	Mn	Sc	Zr	Ti	Be	Fe	Si	Al
1	6.12	0.37	0.26	0.09	<0.03	<0.003	0.09	0.05	Rest
2	4.85	0.32	0.24	0.12	<0.03	<0.003	0.08	0.04	

Note: the averaged chemical composition is given

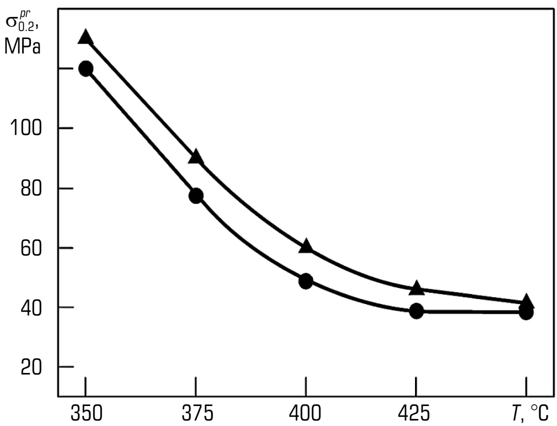

Fig. 1.4 Temperature dependence of yield strength under compression for alloys No. 1 (●) and No. 2 (▲)

As during the test at room temperature [7], at ≤400 °C, a slightly higher resistance to plastic deformation of alloy No. 2 was recorded compared to alloy No. 1, and in the range of 400...450 °C for both alloys it changed slightly (**Fig. 1.4**). Some shift of this dependence for cast alloy No. 2 towards higher temperatures compared to alloy No. 1 can be attributed to the difference in the secondary phase that strengthens the matrix: in alloy No. 2 it is an intermetallic $Al_3(Sc_{1-x}Zr_x)$, and in alloy No. 1 is Al_3Sc [7]. According to literature data, alloys of the Al-Mg-Sc system are processed by thermal deformation in the range of 300...480 °C, although it is recommended to process them at ≤420 °C. Therefore, in order to obtain a wider database, alloys No. 1, 2 were studied after extrusion, pressing and rolling in the range of 390...460 °C (**Table 1.5**).

In the cast state, alloy No. 2 is superior to alloy No. 1 in terms of mechanical characteristics (**Table 1.5**), which significantly increase after deformation treatment: $\sigma_{0.2}$ – from 153...162 to 305...374 MPa; σ_B – from 236...270 to 396...452 MPa; Δ – from 11...15 to 12...17 % depending on its method. The highest strength of alloy No. 1 was obtained after multiple (8 passes) rolling, and for alloy No. 2 – after extrusion. The lower value of σ_B for this alloy after rolling (**Table 1.5**) is probably caused by too high a processing temperature, i.e. the recommendation of an optimal temperature of ≤420 °C for alloys of the Al-Mg-Sc system is confirmed. The obtained results agree with the literature results for similar alloys (**Table 1.5**). It should be noted here that heat-deformed alloys No. 1, 2 show, as a rule, higher values of the yield strength $\sigma_{0.2}$ compared to those known in the literature (**Table 1.5**), which may be a consequence of the use of MHD technology.

● **Table 1.5** Mechanical characteristics of the studied alloys in the cast and thermo-deformed states and their comparison with those known in the literature

Alloy	Processing	$\sigma_{0.2}$, MPA	σ_B, MPa	Δ_5, %
No. 1	Casting	153	236	11
	Extrusion (390 °C)	310	397	12
	Pressing (420 °C)	326	413	13
	Rolling (420 °C)	374	450	12
No. 2	Casting	162	270	15
	Extrusion (420 °C)	350	452	16
	Pressing (420 °C)	309	405	16
	Rolling (460 °C)	305	396	17
01570 [2] (5.8 % Mg)	Extrusion	305…345	430…445	15…18
	Hot rolling	270…300	390…420	15…20
1570 C [2] (5.0…5.6 % Mg)	Pressing and hot rolling	245…300	375…400	15…20
1575 C [16] (6 % Mg)	Rolling (300 °C, ε=70 %)	295	450	20
1545 [16] (4.57 % Mg)	Rolling (360 °C, ε=70 %)	280	385	20
1545 [17] (4.57 % Mg)	Rolling (320...360 °C)	260	395	17
	Cold rolling (ε=20...70 %)	375…450	440…490	8…10

Note: averaged test results of at least three samples are provided for alloys No. 1, 2

The microstructure of alloys after rolling is noticeably different. The grain size transverse to the direction of rolling in alloy No. 1 is 50...150 μm (**Fig. 1.5, *a***), and in alloy No. 2 it is 50...100 μm (**Fig. 1.5, *b***). In alloy No. 1, significant separation of intermetallics along the grain boundaries was recorded, while in alloy No. 2 with a reduced magnesium content, they are much less. Local chemical analysis revealed (**Fig. 1.5, *c, d***) that in both alloys, these are primary allocations of intermetallics: aluminum and magnesium; aluminum, manganese and iron; aluminum, scandium and zirconium (such as Al_3Mg_2, $Al_6(Fe, Mn)$, $Al_3(Sc, Zr)$ [8].

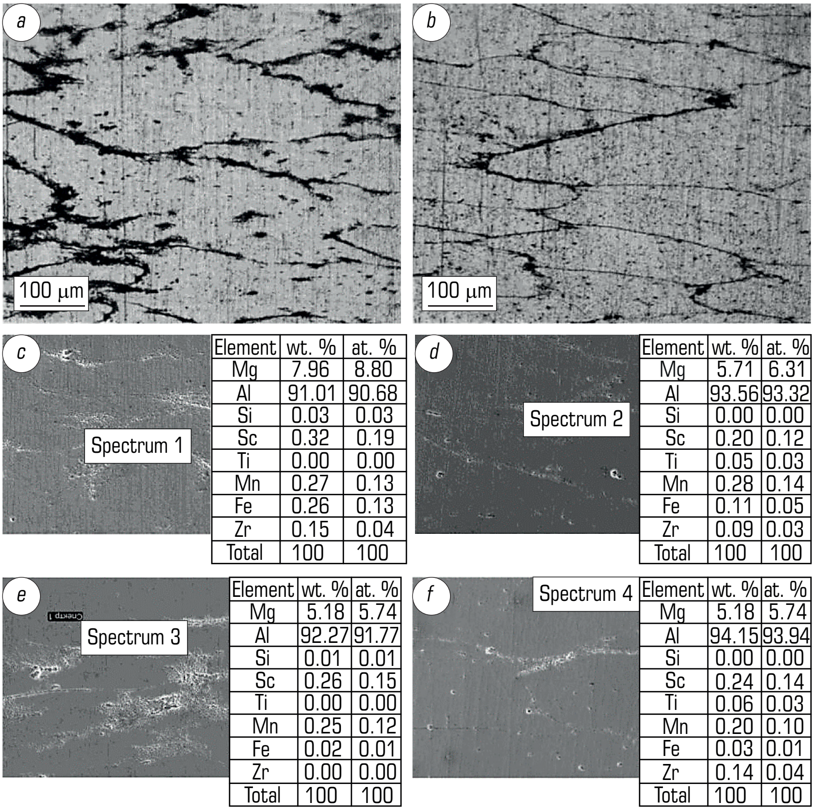

Element	wt. %	at. %
Mg	7.96	8.80
Al	91.01	90.68
Si	0.03	0.03
Sc	0.32	0.19
Ti	0.00	0.00
Mn	0.27	0.13
Fe	0.26	0.13
Zr	0.15	0.04
Total	100	100

Element	wt. %	at. %
Mg	5.71	6.31
Al	93.56	93.32
Si	0.00	0.00
Sc	0.20	0.12
Ti	0.05	0.03
Mn	0.28	0.14
Fe	0.11	0.05
Zr	0.09	0.03
Total	100	100

Element	wt. %	at. %
Mg	5.18	5.74
Al	92.27	91.77
Si	0.01	0.01
Sc	0.26	0.15
Ti	0.00	0.00
Mn	0.25	0.12
Fe	0.02	0.01
Zr	0.00	0.00
Total	100	100

Element	wt. %	at. %
Mg	5.18	5.74
Al	94.15	93.94
Si	0.00	0.00
Sc	0.24	0.14
Ti	0.06	0.03
Mn	0.20	0.10
Fe	0.03	0.01
Zr	0.14	0.04
Total	100	100

Fig. 1.5 Microstructure (*a*, *b*) and local chemical composition of intermetallic compounds (*c*, *d*) and matrix (*e*, *f*) of alloys No. 1 (*a*, *c*, *e*) and No. 2 (*b*, *d*, *f*) after rolling

The difference was found by analyzing their matrix: zirconium is absent in alloy No. 1 (**Fig. 1.5, *e***), while it is present in alloy No. 2 (**Fig. 1.5, *f***). This shows that in the first case, the Al_3Sc secondary phase is released in the matrix, and in the second case, $Al_3(Sc_{1-x}Zr_x)$, which is more dispersed, therefore strengthens the alloy more effectively. A similar result was previously obtained for an alloy with a reduced magnesium content in the cast state [7], as well as other researchers for a heat-deformed alloy [16].

Increased strength of alloys of the Al-Mg-Sc system is achieved, first of all, by alloying with scandium, which structurally strengthens the alloy by grinding the grain, which predicts the Hall-Petch equation. However, it is known that the size of the grain affects the characteristics of strength and CCR ambiguously. In particular, for steels, this dependence for strength and fatigue threshold ΔK_{th} is opposite [18]:

$$\sigma_{0.2} = \sigma_i + k_y D_g^{-0.5}, \tag{1.1}$$

$$\Delta K_{th} = A + BD_g^{0.5}, \tag{1.2}$$

where D_g – the grain size; σ_i, k_y, A, B – material constants. The ΔK_{th} characteristic is important for assessing the durability of structural elements, as it is directly correlated with the resistance to fatigue macrocrack initiation and the fatigue limit of materials [14].

Diagrams of fatigue macrocrack growth rates show (**Fig. 1.6, *a***) that alloy No. 1 after rolling has a somewhat larger CCR in the medium-amplitude part of the diagram and a lower one in the high-amplitude part of the diagram compared to alloy No. 2.

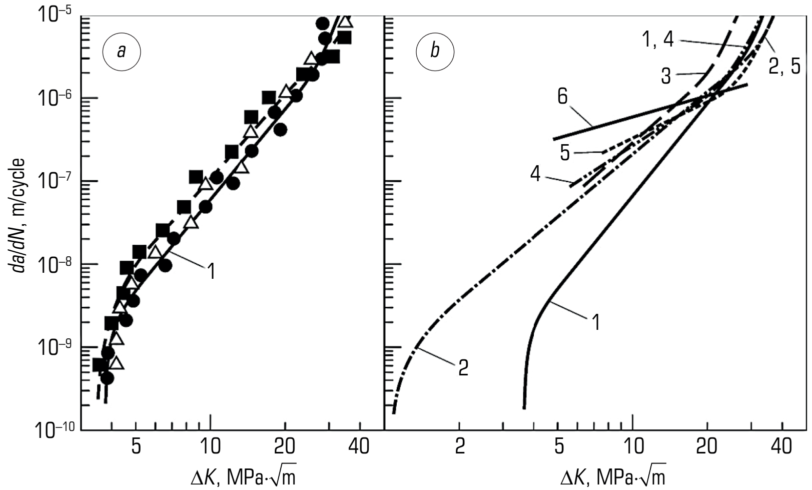

Fig. 1.6 Diagrams of fatigue macrocrack growth rates: *a* – for rolled alloys No. 1 (●, △) and No. 2 (■) under tensile (●) and bending (△, ■) loads; *b* – comparison with literature data for heat-deformed alloys of type 1570: 1 – alloy No. 1, D_g=50...150 μm; 2 – 6...10 μm [12]; 3 – 70...170 μm [9]; 4 – ~1 μm [9]; 5 – [3]; 6 – [2]

Note that the diagram for alloy No. 1 (similar to the known results [19]) is invariant with respect to the geometry and method of sample loading, that is, it is a characteristic of the material. Both alloys have a high resistance to fatigue macrocrack growth, which is caused by high-energy micro-mechanisms of destruction: at $\Delta K \approx 15$ MPa$\cdot\sqrt{\text{m}}$, this is a fatigue groove (**Fig. 1.7, *a*, *b***); at $\Delta K \approx 25$ MPa$\cdot\sqrt{\text{m}}$ – it is mainly pitted (**Fig. 1.7, *c*, *d***).

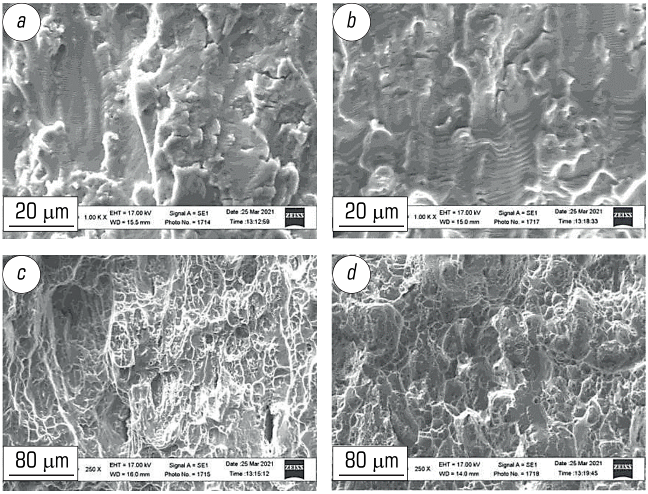

Fig. 1.7 Microfractograms of samples from alloys No. 1 (*a*, *c*) and No. 2 (*b*, *d*) at $\Delta K=15$ (*a*, *b*) and 25 MPa$\cdot\sqrt{\text{m}}$ (*c*, *d*)

Both alloys with a relatively large grain size ($D_g=50...150$ μm) show a relatively high fatigue threshold $\Delta K_{th}=3.3...3.8$ MPa$\cdot\sqrt{\text{m}}$, which distinguishes them from the known ones (**Fig. 1.6, *b***, line 1 vs. 2): for alloy 1570 with a small grain size ($D_g=6...10$ μm) $\Delta K_{th}=1.1$ MPa$\cdot\sqrt{\text{m}}$ [12], which confirms the above considerations. In the high-amplitude region ($\Delta K=15...30$ MPa$\cdot\sqrt{\text{m}}$), these diagrams agree well with the results of other authors (**Fig. 1.6, *b***). They also show (lines 4 and 6) that alloys with fine grain ($D_g \sim 1$ μm) show low CCR in the low-amplitude region of the diagram ($\Delta K < 5$ MPa$\cdot\sqrt{\text{m}}$). Therefore, taking into account the ambiguous influence of the structure on the strength and CCR of alloys of the Al-Mg-Sc system, their mechanical behavior under operating conditions should be evaluated according to the above structural strength parameter *P* (**Table 1.6**).

Among the aluminum alloys of different alloying systems, alloy No. 1 has the highest value of the *P* parameter, and alloy No. 2 has the lowest value, although it is practically equal to the high-strength D16T alloy, but it is higher compared to the medium-strength AMg_5M alloy, which is widely used in aerospace engineering. Note that the fine-grained structure of the alloy, causing a very low fatigue threshold ΔK_{th}, determines the lowest value of the *P* parameter, despite the relatively high strength of this alloy (item 3 in **Table 1.6**).

Table 1.6 Mechanical characteristics and parameter of structural strength of aluminum alloys

No.	Alloy (alloying system)	Alloy condition	σ_B, MPa	ΔK_{th}, $\text{MPa}\cdot\sqrt{\text{m}}$	ΔK_{fc}, $\text{MPa}\cdot\sqrt{\text{m}}$	*P*, $\text{MPa}^3\cdot\text{m}$
1	No. 1 (Al-Mg-Sc)	Hot rolling	450	3.8	33	56430
2	No. 2 (Al-Mg-Sc)	–||–	396	3.4	35	47124
3	01570 [12] (Al-Mg-Sc)	Hot rolling, annealing	410	1.1	35	15785
4	AMg5M [20] (Al-Mg)	–||–	315	3.2	33	33264
5	D16M [20] (Al-Cu-Mg)	–||–	235	3.5	32	26320
6	D16T [20] (Al-Cu-Mg)	Hot rolling, hardening, natural age hardening	415	3.2	34	45152

Thus, in order to achieve increased structural strength, alloys of the Al-Mg-Sc system should have an average grain size, obviously several tens of micrometers.

1.3 THE INFLUENCE OF RARE-EARTH METALS ON THE STRUCTURE AND PROPERTIES OF CAST AND DEFORMED ALLOYS OF THE Al-Mg-Cr-Sc-Zr SYSTEM

It was revealed that the Al-Mg-Sc system alloy, which has a reduced magnesium content (4.55...4.65 wt. %) and instead of manganese contains 0.4...0.5 wt. % chromium, in terms of corrosion and mechanical characteristics, the well-known alloy 1545 prevails, but it also needs to increase the strength in the cast state.

Considering the high cost of scandium, an effective means of influencing the structure and physical and mechanical properties of alloys of the Al-Mg-Sc system is microalloying with rare-earth metals (REM). Having a specific electronic structure of the d-shell and the size of the atom, they are able to form complex alloyed solid solutions and intermetallics in these alloys, which contributes to grain grinding, increasing the purity of grain boundaries, increasing microhardness, and improving their mechanical and corrosion properties. First of all, this applies to erbium and lanthanum [21–26]. It was established that lanthanum is most similar to scandium in its effect [26], and the effectiveness of erbium is low at reduced scandium content [25]. It is believed that ~0.10 wt. % is the optimal content of erbium or lanthanum in the alloys of this system [21, 26].

The effect of erbium and lanthanum on the structure, phase composition, and mechanical and corrosion properties of an alloy of the Al-Mg-Sc system, in which the magnesium content is reduced and manganese is replaced by chromium, was studied after plastic deformation of castings obtained by MHD technology [27]. The well-known alloy 1545 with a reduced magnesium content (No. 1 in **Table 1.7**) was chosen as the base. In alloys No. 2, 4–7, manganese is replaced by chromium to increase corrosion resistance [7]. The effect of erbium was studied on alloys No. 3, 4, and lanthanum on alloys No. 5–7.

Table 1.7 Chemical composition (wt. %) of the investigated alloys

Alloy No.	Mg	Mn	Cr	Sc	Zr	Er	La	Fe	Si
1	4.64	0.43	–	0.28	0.09	–	–	0.21	0.16
2	4.70	–	0.45	0.26	0.13	–	–	0.14	0.10
3	4.62	0.36	–	0.28	0.12	0.06	–	0.11	0.14
4	4.72	–	0.49	–	0.35	0.15	–	0.22	0.12
5	4.67	–	0.45	0.25	0.12	–	0.08	0.10	0.07
6	4.65	–	0.40	0.15	0.10	–	0.11	0.11	0.09
7	4.63	–	0.42	0.10	0.1	–	0.25	0.10	0.10

Note: the averaged chemical composition is given; all alloys also contain ~0.03 wt. % Ti and ~0.003 wt. % Be, the rest – Al

Castings were obtained by MHD mixing of the melt at 700±10 °C and crystallization in a steel mold at 20 °C and heated to 300 °C for the initial homogenization of the casting structure. Castings were homogenized at 360 °C for 5 hours with cooling in water or in air at 20 °C.

Considering that the temperature of 360 °C is optimal for thermo-deformation processing of alloys of the Al-Mg-Sc system [25, 28, 29], the homogenized castings were pressed at this temperature into strips 12 mm thick and then rolled into plates 6 mm thick. After annealing at 360 °C for 1 hour they were thinned by cold rolling first to a thickness of 4 mm and annealed at 200 °C for 1 hour, and then to a thickness of 2 mm and also annealed at 200 °C for 1 hour.

Cast alloys. An increase in the mechanical characteristics $\sigma_{0.2}$ and σ_B was recorded after replacing manganese with chromium in alloys with a reduced (4.64...4.70 wt. %) magnesium content (No. 1, 2 in **Table 1.8**), which was associated with the intensification of the release of intermetallics $Al_3(Sc_{1-x}Zr_x)$. Doping with erbium (0.06 and 0.15 wt. %) of alloys with manganese or chromium led to a decrease in strength characteristics, which increases with an increase in the content of erbium (up to 0.15 wt. %) and zirconium (up to 0.35 wt. %) in the absence of scandium (No. 3, 4 vs. No. 1, 2). In the paper [25], they also did not find a positive effect of erbium on the mechanical properties of the thermoformed alloy of the Al-Mg-Mn-Sc-Zr system when it was reduced from 0.25 to 0.12 wt. % of scandium content.

Doping with lanthanum (0.08 wt. %), on the contrary, leads to an increase in strength characteristics with a slight decrease in plasticity (No. 5 vs. No. 2). At the same time, as with erbium doping, increasing the lanthanum content (up to 0.11...0.25 wt. %) with a reduced (from 0.25 to 0.10...0.15 wt. %) scandium content does not have a positive effect: strength decreases significantly with increasing plasticity (No. 6, 7 vs. No. 5). However, it should be noted here that with a 2.5-fold reduction in the content of precious scandium after alloying with lanthanum, a highly plastic and sufficiently strong alloy was obtained in the cast state (No. 7 vs. No. 5).

Table 1.8 Mechanical characteristics of the studied alloys in the cast state

Characteristics	Alloy No.						
	1	**2**	**3**	**4**	**5**	**6**	**7**
$\sigma_{0.2}$, MPa	162	175	152	132	204	152	132
σ_B, MPa	270	280	260	248	292	255	250
Δ_5, %	16	15	17	18	12	21	22

Note: alloy number according to **Table 1.7***; averaged test results of 3–5 samples are given*

Next, alloy No. 5 was studied. The structure and properties of the cast metal depend on the cooling rate during crystallization and after homogenization of the casting. It was established (**Table 1.9**) that during its growth during the crystallization of the casting (mold at a temperature of 20 °C versus heated to 300 °C), the microhardness of the grain body and the strength characteristics of alloy No. 5 decrease somewhat. The mechanical properties of the casting obtained in a mold heated to 300 °C improve after homogenization at 360 °C. At the same time, they also depend on the speed of cooling after homogenization: they increase more significantly when it is lower, that is, during cooling in air. As the homogenization temperature increases to 420 °C, the microhardness and strength characteristics decrease (**Table 1.9**).

Table 1.9 Influence of the cooling rate and homogenization of castings on the mechanical characteristics of alloy No. 5

Alloy condition	$HV_{0.1}$, **GPa**	$\sigma_{0.2}$, **MPa**	σ_B, **MPa**	Δ_5, **%**
Cast (molded at 300 °C)	0.74	204	292	12
Cast (molded at 20 °C)	0.69	200	285	14
Homogenization (360 °C, cooled in water)	1.00	225	310	12
Homogenization (360 °C, cooled in air)	1.05	240	320	13
Homogenization (420 °C, cooled in air)	0.85	209	281	12

Note: averaged values based on the results of 3–5 measurements are given; the microhardness of the grain body was determined

The change in the mechanical characteristics of alloy No. 5 correlates with the features of its microstructure. After crystallization in a heated mold, there is a non-dendritic structure with a grain size of 50...100 μm with the release of intermetallics of the Al_3Mg_2 type [30] along the grain boundaries (**Fig. 1.8, *a***), which worsen the mechanical properties. Therefore, the decrease in the strength of the alloy after crystallization in the mold at 20 °C (**Table 1.9**) is caused by the more intense release of these intermetallics (**Fig. 1.8, *b***), even with a certain decrease (to 50...70 μm) in the grain size. The growth of the $HV_{0.1}$, $\sigma_{0.2}$ and σ_B characteristics of the alloy after homogenization during cooling in water (**Table 1.9**) can be associated with the separation of the secondary phase in the body of the grain (**Fig. 1.8, *c***). At the same time, as there are more discharges after homogenization with air cooling (**Fig. 1.8, *d***), the mechanical characteristics of the alloy increase significantly (**Table 1.9**).

Local chemical analysis shows (**Table 1.10**) that for the highest strength characteristics of alloy No. 5 after crystallization in a mold heated to 300 °C and homogenization with cooling in air (**Table 1.10**) with an almost unchanged content of the main alloying elements (Mg, Cr, Sc, Zr, and Ti) in the matrix and intermetallics, the content of lanthanum changes noticeably: it decreases by three times in the primary intermetallics along the grain boundaries and increases by the same number of times in the matrix and secondary intermetallics in the body of the grain. Thus, microalloying with lanthanum (~0.1 wt. %) can increase the strength of the cast alloy of the Al-Mg-Cr-Sc-Zr system by dispersion strengthening with secondary intermetallics of the types Al_3La [24], $Al_3(Sc_{1-x}P3M_x)$ [31], $(Al, Cr)_3(Zr, REM)$ [32] after homogenization of the casting.

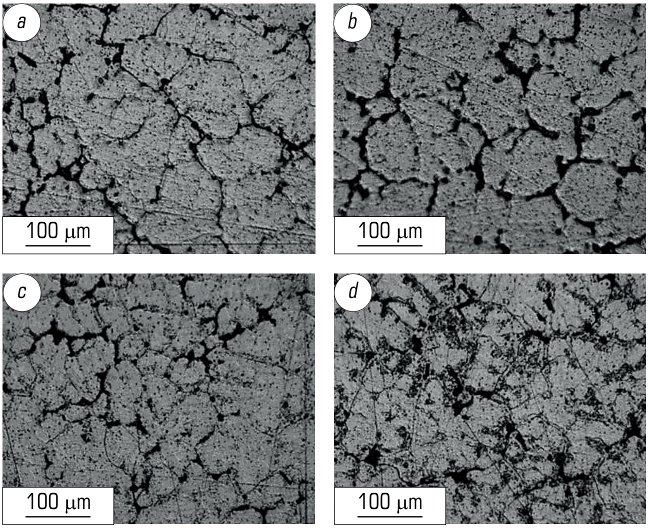

Fig. 1.8 Microstructure of alloy No. 5 depending on the cooling rate during crystallization (*a*, *b*) and after homogenization (*c*, *d*) casting: *a*, *b* – mold at 300 °C and 20 °C; *c*, *d* – cooling in water and air

Table 1.10 Local content of alloying elements in castings of alloy No. 5 (mold at 300 °C, homogenization at 360 °C, cooled in air)

Structural zone	Alloy condition	Elements, wt. %								
		Mg	Cr	Sc	Zr	La	Ti	Fe	Si	Al
Matrix	Cast	3.75	0.55	0.26	0.29	0.03	0.05	–	–	Rest
	After homogenization	3.62	0.54	0.23	0.26	0.11	0.08	0.03	–	–‖–
Intermetallics	Cast	7.55	0.29	0.31	0.11	0.15	0.02	0.28	0.10	–‖–
	After homogenization	6.95	0.35	0.36	0.10	0.05	0.02	0.17	0.06	–‖–

Note: The average content is given based on the results of 3–5 measurements

Deformed alloys. The effect of hot and cold plastic deformation was studied on castings of alloy No. 5 after crystallization in a mold heated to 300 °C and homogenization at 360 °C for 5 hours with air cooling, which demonstrated the highest mechanical properties (**Table 1.10**).

It has an anisotropic microstructure traditional for rolled materials, where the grains are elongated along the direction of rolling (**Fig. 1.9**), and their size depends on the mode of deformation processing of the samples: it is 10...30 μm for hot-rolled ones (**Fig. 1.9, *a***) and 10...15 μm (**Fig. 1.9, *b***) and 5...10 μm (**Fig. 1.9, *c***) – for cold-rolled ones with a thickness of 4 and 2 mm, respectively. Note that after cold rolling, the primary intermetallics are crushed and their shape is mostly globular. The size of intermetallic inclusions is 1...5 μm and they are fairly evenly located in the volume of the material (**Fig. 1.9, *d***).

Local chemical analysis shows that, compared to the cast state (**Table 1.10**), in the deformed alloy No. 5 (**Table 1.11**), the qualitative picture of the distribution of the main alloying elements in the matrix and intermetallics is similar. But the content of magnesium, chromium, scandium and zirconium increases in the intermetallics of the deformed alloy. At the same time, the concentration of alloying elements in the matrix, except for zirconium, is practically the same as in castings after homogenization. This also applies to lanthanum, i.e. secondary allocations of Al-Sc-Zr, Al-La or Al-Cr-Zr-La systems are preserved in the matrix of the deformed alloy [32]. In addition, chromium and titanium are found in the solid solution of the matrix. Thus, based on the results of these analyses, it can be stated that deformed alloy No. 5 should have high mechanical characteristics due to structural (grain crushing), solid-solution and dispersion strengthening.

Compared with castings after homogenization (**Table 1.9**), the strength of alloy No. 5 after hot pressing and rolling increases by 20...23 % with the same plasticity (**Table 1.12**). After cold rolling, this tendency increases significantly: compared to the cast state, the yield strength increases by 1.6–1.8 times, depending on the degree of deformation, and the strength limit by 1.3–1.5 times. Annealing after rolling slightly reduces these characteristics due to the increase in plasticity of the alloy, although they remain sufficiently high. The obtained characteristics of deformed alloy No. 5 are at the level of the best-known results for alloys 1570 and 1545 (**Table 1.12**).

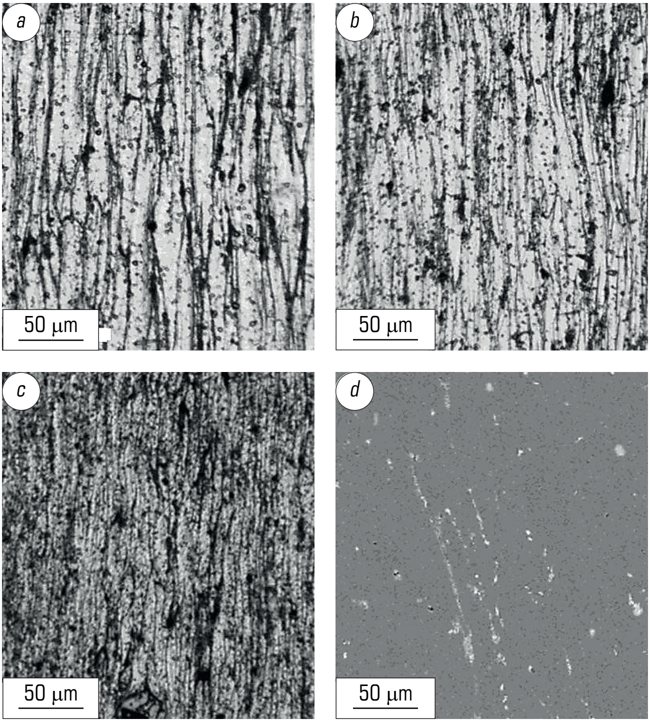

Fig. 1.9 Microstructure of alloy No. 5 after hot (*a*) and cold rolling of samples with a thickness of 4 mm (*b*, *d*) and 2 mm (*c*); *d* – electron microscopy

Table 1.11 Local content (wt. %)* of the main alloying elements in deformed alloy No. 5

Processing	Structural zone	Mg	Cr	Sc	Zr	Ti	La
Hot rolling	M	3.57	0.41	0.23	0.11	0.03	0.12
	I	10.14	14.51	0.80	0.46	–	0.05
Cold rolling	M	3.48	0.42	0.24	0.14	0.04	0.11
	I	10.10	14.95	0.51	0.37	0.01	0.03

*Note: * averaged data of 3–5 measurements; M – matrix; I – intermetallics*

Table 1.12 Mechanical characteristics of deformed alloy No. 5 and their comparison with those known in the literature

Alloy	Processing (plate thickness, mm)	$\sigma_{0.2}$, MPa	σ_B, MPa	Δ_5, %
No. 5	HR(12)	280	378	14
	HR(6)	292	395	13
	HR(6)+A_1	283	380	16
	CR(4)	385	423	8
	CR(4)+A_2	350	418	13
	CR(2)	430	472	7
	XB(2)+A_2	361	422	10
01570 [33]	HR*(5)	297	376	7
	CR(3)	429	470	5
	CR(3)+A*	312	383	14
P-1580 [33]	HR*(5)	312	389	12
	CR(3)	409	453	5
	CR(3)+B*	277	390	14
1545 [17]	HR (320…360 °C)	260	395	17
	CR (ε=20…70 %)	375…450	440…490	8…10

Note: 1 hour; HR* – at 450 °C; A* – at 350 °C, 3 hours; ε_i – the deformation value; averaged test data of 3–5 samples are presented

Deformed alloy No. 5, in which the magnesium content is reduced and manganese is replaced by chromium with additional microalloying with lanthanum, similar to the cast state, has higher corrosion resistance compared to deformed alloys 1570 and 1545 (**Fig. 1.10, *c*** vs. **Fig. 1.10, *a*, *b***).

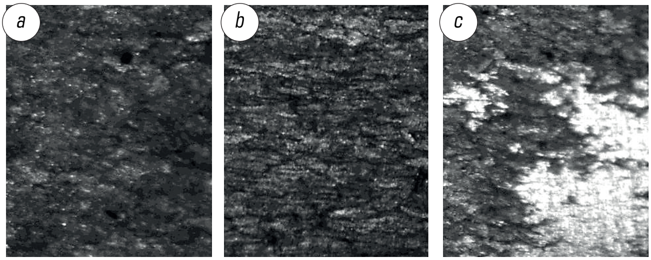

E_{cor}=–873 mV I_{cor}=8.4 mA/m^2 | E_{cor}=–752 mV I_{cor}=6.5 mA/m^2 | E_{cor}=–716 mV I_{cor}=3.6 mA/m^2

Fig. 1.10 The corroded surface of samples of hot-rolled alloys 1570 (*a*), 1545 (*b*) and No. 5 (*c*) and their electrochemical characteristics

Its electrochemical characteristics are better: the corrosion potential E_{cor} increases, and the corrosion current I_{cor} decreases. This is due to the positive effect of lanthanum [34], in addition to chromium [7], on cleaning the grain boundaries and improving the electrochemical potential.

Structural strength of alloys. The performance of materials, when the principle of safe damage is applied during their operation, depends on the optimal combination of strength characteristics and CCR, so it can be effectively evaluated by the complex parameter of structural strength *P*. Increasing the strength of alloys of the Al-Mg-Sc system is achieved, first of all, by alloying with scandium, which structurally strengthens them by grinding the grain. However, its size has the opposite effect on the strength and CCR of materials: the strength increases according to the Hall-Petch equation, and the fatigue threshold ΔK_{th} decreases [15, 35].

The obtained diagrams of fatigue macrocrack growth rates show (**Fig. 1.11, *a***) that alloy No. 5 after various treatments has high CCR characteristics, especially in the high-amplitude region, when $\Delta K_{fc} \approx 50$ MPa $\cdot \sqrt{\text{m}}$.

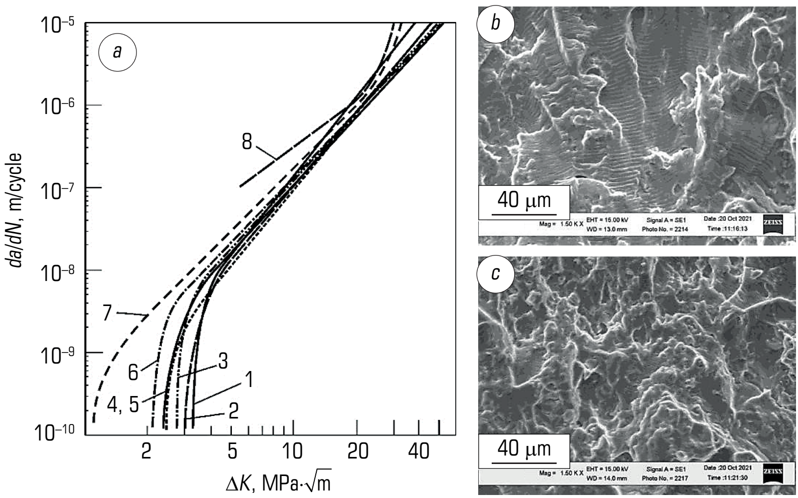

⬡ **Fig. 1.11** Diagrams of fatigue macrocrack growth rates (*a*) in alloy No. 5:
1 – HR(6), D_g=10…30 μm; 2 – HRV(6)+A_1; 3 – CR(4), D_g=10…15 μm; 4 – CR(4)+A_2;
5 – CR(2), D_g=5…10 μm; 6 – CR(2)+A_2 (designation see **Table 1.12**) and their comparison with literature results for deformed alloys of type 1570: 7 – $D_g \approx 6$ μm [12]; 8 – $D_g \approx 1$ μm [3], as well as microfractograms of samples of alloy No. 5 after CR (*b*) and CR (*c*) at $da/dN \approx 1.10^{6}$ m/cycle

Annealing after hot and cold rolling leads to a slight decrease in the fatigue threshold ΔK_{th} and an increase in the cyclic fracture toughness ΔK_{fc} (curve 2 vs. curves 1, 4 vs. curve 3, and curve 6 vs. curve 5). The smaller grain size of the material after cold rolling compared to hot rolling (**Fig. 1.9**) leads to a decrease in the fatigue threshold ΔK_{th} (curves 3 and 5 versus 1), i.e., here the trend is opposite to the change in strength characteristics (**Table 1.12**). This regularity is confirmed by the results for other alloys of the Al-Mg-Sc system (**Fig. 11, *a***): with a grain size of 1...6 μm, they have a lower CCR, especially in the threshold area (curves 7, 8), compared to alloy No. 5 with grains 5...30 μm after various treatments (curves 1–6).

The high CCR characteristics of alloy No. 5, in particular the cyclic fracture toughness ΔK_{fc}, are due to the implementation of energy-intensive micromechanisms of viscous fracture: classic grooved after hot rolling (**Fig. 1.11, *b***) and pitted with the formation of deformation ridges after cold (**Fig. 1.11, *c***).

As a result, the structural strength parameter *P* of various modifications of alloy No. 5 is quite high (**Table 1.13**): after hot rolling and annealing, it is ~4 times greater than for the fine-grained alloy 01570, and compared to the D16T alloy widely used in aerospace engineering, it is ~1.3 times. Alloy No. 5 surpasses this alloy in terms of the *P* parameter also in the state after cold rolling (**Table 1.13**), when it has the highest (472 MPa) strength.

Table 1.13 Mechanical characteristics and parameter of structural strength of aluminum alloys

Alloy	Processing	σ_B, MPa	ΔK_{th}, MPa·$\sqrt{m}$	ΔK_{fc}, MPa·$\sqrt{m}$	*P*, MPa^3·m
No. 5, D_g=3…30 μm	HR(6)	395	3.2	38	48030
	HR(6)+A_1	380	3.0	52	59280
	CR(4)	423	2.7	49	55960
	CR(4)+A_2	418	2.4	51	51160
	CR(2)	472	2.4	46	52110
	CR(2)+A_2	422	2.1	50	44310
01570, D_g=6…10 μm [15]	HR+A	410	1.1	35	15790
D16T [15]	HR+hardening and age hardening	415	3.2	34	45150

Note: designation see **Table 1.12**

Therefore, the alloy of the Al-Mg-Cr-Sc-Zr-La system in the cast state has increased strength characteristics after crystallization in a mold heated to 300 °C and homogenization at 360 °C with cooling in air due to additional dispersion strengthening with lanthanum intermetallics. After hot (at 360 °C) and cold rolling, it is not inferior in terms of strength and plasticity to known alloys of the Al-Mg-Mn-Sc-Zr system (grades 1570 and 1545), but it surpasses them in terms of corrosion resistance, which is due to the positive influence of lanthanum and chromium for cleaning the grain boundaries and refining the electrochemical potential, as well as for the characteristics of cyclic crack resistance.

1.4 PRESSING OF SEMI-FINISHED PRODUCTS FROM ALLOYS OF THE Al-Mg-Sc SYSTEM IN ISOTHERMAL CONDITIONS

Aluminum alloys can be significantly strengthened by deformation processing, in particular, hot pressing, hot and cold rolling, etc. However, with the selection of suboptimal temperature and force parameters of such processing, micro- and macro-damage is formed in semi-finished products from these alloys, especially in the near-surface layers, due to which the physico-mechanical properties of the deformed metal deteriorate. Therefore, let's study how to optimize the temperature-force parameters of hot pressing in isothermal conditions of a cast cylindrical billet from alloys of the Al-Mg-Sc system in order to form strips of different thicknesses with minimal damage [36].

Let's study castings from alloys 1570 and 1545 (**Table 1.14**), which were obtained after crystallization in a steel mold preheated to 300 °C. At the same time, the melt at 700±10 °C was subjected to magnetohydrodynamic stirring. Therefore, the castings were not homogenized.

Table 1.14 Average chemical composition of alloys

Alloy	Element content, wt. %						
	Mg	**Mn**	**Sc**	**Zr**	**Fe**	**Si**	**Al**
1570	5.96	0.40	0.24	0.09	0.28	0.16	Rest
1545	4.61	0.43	0.28	0.12	0.31	0.17	–||–

The pressing temperature was chosen based on the results of standard compression tests of samples and it was found that the temperature dependences of the yield strength of alloys 1570 and 1545 are qualitatively similar (**Table 1.15**). Let's took into account, on the one hand, the temperature at which a sharp drop in the resistance to plastic deformation of the samples begins, and on the other hand, the need to reduce the processing temperature, therefore, a pressing temperature of 360±5 °C was adopted for both alloys.

Table 1.15 Temperature change in yield strength (MPa) of alloys during compression tests

Alloy	Test temperature, °C						
	150	**250**	**350**	**375**	**400**	**425**	**450**
1570	139	130	120	75	50	40	40
1545	149	139	130	90	60	47	40

Note: average test results of 3–5 samples are given

Simulation of pressing was carried out in the DEFORM3D software complex [37] and full-scale pressing of cast blanks. The correctness of the calculations was assessed by comparing them with the experimentally determined force parameters. The cylindrical workpiece 1 (∅ 30 mm and length 50 mm) cut from the casting was pressed through the matrix 2 by the punch 3 with the output of a strip 4 with a width of 30 mm and a given thickness (**Fig. 1.12, *a***).

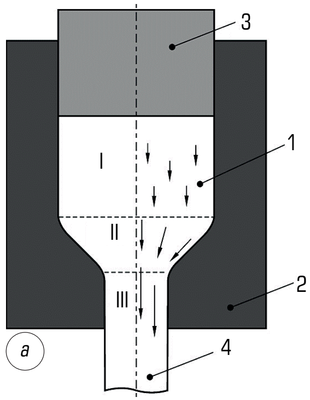

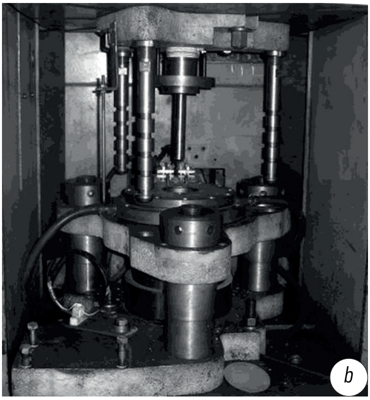

Fig. 1.12 Calculation scheme (*a*) and general view of the hot pressing installation (*b*): I, II, III – deformation zones. The arrows point to the movement speed vectors (the length of the arrow is proportional to the movement speed)

It was assumed that the matrix and punch are absolutely rigid and the Siebel law of contact friction is fulfilled, and the following initial data were also accepted: Coulomb friction coefficient $\mu=0.1...0.5$; temperature of the workpiece and tools $t=360$ °C; speed of the deforming tool $V_0=5$ mm/s; the model material is aluminum alloy 5056 (similar to the investigated alloys in terms of deformation properties).

Natural isothermal hot pressing of the strip was carried out on a PD-476 hydraulic press (**Fig. 1.12, *b***), the working unit of which was heated to the selected temperature. Process parameters (force, punch speed and temperature) were monitored by appropriate sensors with computer recording. The workpieces were heated to the specified temperature in an electric furnace SNOL 30/1300 with an error of ±5 °C.

The general field of metal movement velocities at the time of establishment of a stable pressing mode can be conditionally divided into three characteristic zones (**Fig. 1.12, *a***): I – here the workpiece retains its cylindricality, the speed along the *Z* and *Y* axes is uniform and equal to the punch movement speed; the size of this zone is variable and depends on the distance of the plane of the face of the punch to the point where the narrowing of the matrix channel begins; II – the zone from the beginning of the narrowing of the matrix channel to the calibration hole; here, the largest deformations occur and a structure with the corresponding properties of the strip material is formed, which is calibrated in zone III.

In the II zone, the velocity vectors change the direction of movement of the metal particles depending on the profile of the cone of the matrix. Due to the symmetry of the cross-section of the workpiece, two streams of metal meet here, which increases the speed of movements in this place. Therefore, their distribution along the Y axis is uneven: the maximum speed value is on the axis of symmetry, and the minimum value is on the working contour of the matrix profile. This is confirmed by the results of the calculation of deformation rates, the intensity distribution of which is shown in **Fig. 1.13** for a stable pressing mode. The maximum rate of deformation is characteristic of the center of zone II in sections *ZY* and *XZ*. At the same time, it decreases along the *X* coordinate in the *XZ* section to the working contour of the matrix. As a result of this distribution of velocities along the strip thickness, a zone of residual deformations with a value of 0.95…1.0 is formed in the middle along the *Z* axis, which decrease towards the edge of the strip (along the *X* coordinate) to 0.75…0.8. Along the *Z* axis, the values and distribution of deformations practically do not change. An exception is the zone of entry of the cylindrical workpiece into the working calibration part of the matrix and the exit of the workpiece. The non-uniformity of the intensity of deformations in the cross-section of the strip reaches 15…17 %.

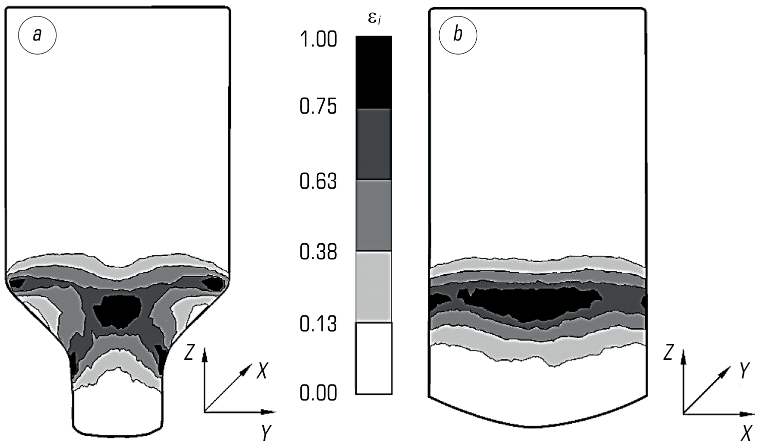

Fig. 1.13 Distribution of the intensity of deformation rates ε_i at the moment of establishment of a stable pressing mode: *a* – in the *ZY* plane; *b* – in the *XZ* plane

Along the thickness of the band in the cross-section *ZY*, the distribution of deformations is more complicated due to the occurrence of significant shear deformations in zone II on inclined conical surfaces (**Fig. 1.14, *a***). As a result, their intensity sharply increases on the calibration surfaces of the matrix (**Fig. 1.14, *b*, *c***).

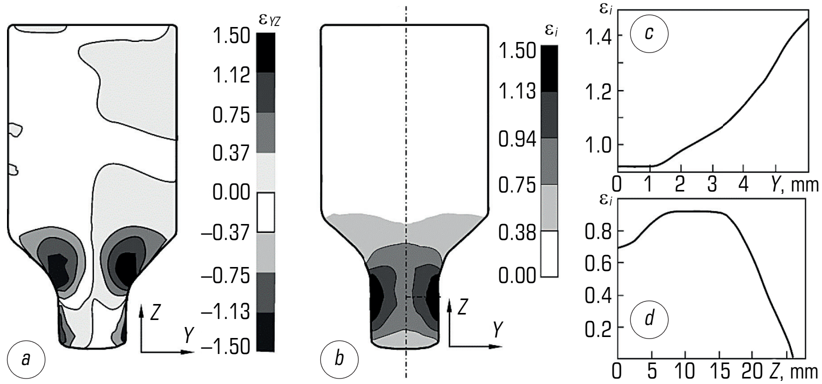

Fig. 1.14 Shear deformations ε_{yz} (*a*) and the distribution of their intensity according to Mises at the time of establishment of a constant deformation force (*b*), in particular, in sections *ZY* along the *Y* axis (*c*) and *ZY* along the *Z* axis (*d*)

The calculation showed that after pressing, the distribution of the intensity of the residual deformations along the thickness of the strip is uneven, which was confirmed experimentally. The grain size of the material in the cross-section of the strip varies noticeably: in the near-surface zone it is ~2 times smaller than in the middle (**Fig. 1.15**), which corresponds to the nature of the influence of the intensity of deformations on the conditions of recrystallization of the deformed grain during hot pressing.

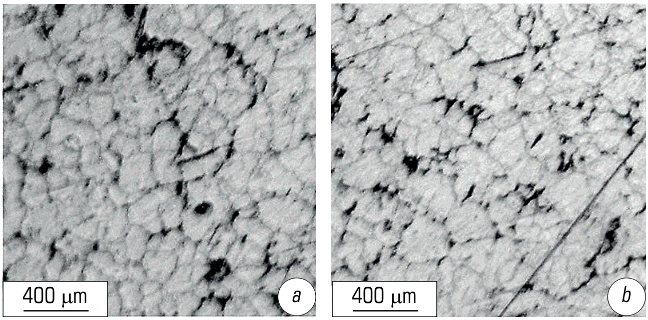

Fig. 1.15 Change in the microstructure of alloy 1570 along the strip thickness: *a* – near-surface zone; *b* – the middle

By comparing calculated and experimental values of force during hot pressing of the strip, it was found (**Fig. 1.16**) that with a friction coefficient of $\mu=0.5$, the error of the calculated compared to the actual value does not exceed 20...22 %. By reducing the friction coefficient to 0.1...0.3, it is possible to significantly weaken the pressing force (curves 4 and 5 in **Fig. 1.16**), which is achieved by using high-temperature lubricant on the surfaces of the workpiece and matrix.

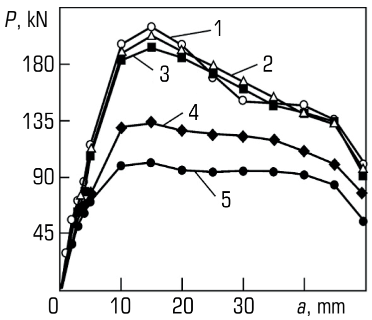

Fig. 1.16 Comparison of the dependences of the pressing force *P* on the displacement a of the punch, determined experimentally for blanks made of alloys 1545 (curve 1) and 1570 (curve 2), and calculated: 3 – μ=0.5; 4 – 0.3; 5 – 0.1

It was established that the average compressive stress on the surface of the calibration belt reaches 110...120 MPa, which exceeds the yield point of the material at the pressing temperature (**Table 1.15**), i.e., destruction due to deformational damage may occur here. In the phenomenological theory of destruction [38], damageability ω is taken as the calculation parameter. Taking into account that the deformations during pressing are monotonous, a linear model in the form of:

$$\omega = \int_t \frac{\dot{\varepsilon}_i dt}{\Lambda_p\left(\Pi_\sigma, \mathrm{T}\right)}, \tag{1.3}$$

where ε_i – the intensity of deformation rates; t – deformation time; $\Lambda_p\left(\Pi_\sigma, \mathrm{T}\right)$ – metal fracture deformation; Π_σ – load stiffness index; T – the temperature of the metal during deformation. Here,

$$\Pi_\sigma = \frac{3\sigma_m}{\sigma_i}, \tag{1.4}$$

where $\sigma_m = 1/3\left(\sigma_1 + \sigma_2 + \sigma_3\right)$ – average tension; σ_i – stress intensity. The deformation of metal fracture at a given process temperature was determined on samples under uniaxial tension. This approach gives estimated results, the error of which does not exceed 15–20 %.

It was believed that in the initial state of the metal (before deformation) ω=0; at the time of band destruction ω=1. Intermediate values of ω determine the accumulation of micro- and macro-defects in the metal. Some threshold values of damage were established [39, 40–42]: $0 \le \omega \le 0.2$, when deformation defects disappear after recrystallization annealing; 0.2...0.4≤ω≤0.6...0.8 – microdefects are formed in the metal that are not healed during heat treatment, and the metal loses its bearing capacity (mechanical characteristics decrease); ω>0.6...0.8 – there is a possibility of metal destruction.

The calculated distribution of damage – ω=0.35...0.45, and with a decrease in thickness to 6 mm – ω=0.50...0.55. At the same time, it was experimentally recorded that in the first case the strip is without visible defects, and in the second – with surface macrocracks.

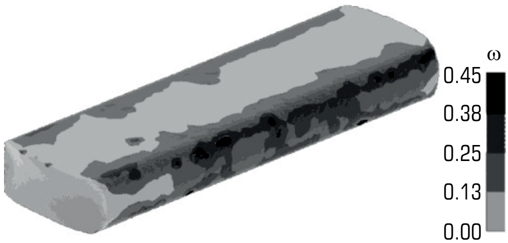

Fig. 1.17 Distribution of damage ω in a strip with a thickness of 12 mm

Therefore, for the optimized selection of geometric parameters of the strip and equipment for pressing, it is proposed to determine the calculated damage rate ω at the process design stage. It was found that at ω=0.35...0.45 there is no visually observable crack formation, and when this parameter increases (ω=0.50...0.55), macrocracks appear on the strip surface.

CONFLICT OF INTEREST

The authors declare that they have no conflict of interest in relation to this research, whether financial, personal, authorship or otherwise, that could affect the research and its results presented in this paper.

REFERENCES

1. Ostash, O. P., Fedirko, V. M., Uchanin, V. M., Bychkov, S. A., Moliar, O. H., Semenets, O. I. (2007). Mitsnist i dovhovichnist aviatsiinykh materialiv ta elementiv konstruktsii. Lviv: SPOLOMb, 1068.
2. Filatov, Yu. A., Yelagin, V. I., Zakharov, V. V. (2000). New Al-Mg-Sc alloys. Materials Science and Engineering: A, 280 (1), 97–101. doi: https://doi.org/10.1016/s0921-5093(99)00673-5

3. Li, M., Pan, Q., Wang, Y., Shi, Y. (2014). Fatigue crack growth behavior of Al-Mg-Sc alloy. Materials Science and Engineering: A, 598, 350–354. doi: https://doi.org/10.1016/j.msea.2014.01.045
4. Fernandes, M. T. (2001). Pat. PCT/US00/19559. Aluminium-magnezium-scandium alloys with hafnium. Publ. 22.02.2001.
5. Polyvoda, S. L., Siryi, O. V., Hordynia, O. M., Puzhailo, L. P. (2017). Pat. No. 119406 UA. Plavylno – lyvarnyi kompleks dlia napivbezperervnoho lyttia zlyvkiv z aliuminiievykh splaviv. MPK B22D 11/14. No. u201703178; declareted: 03.04.2017; published: 25.09.2017, Bul. No. 18. Available at: https://uapatents.com/5-119406-plavilno-livarnijj-kompleks-dlya-napivbezperervnogo-littya-zlivkiv-z-alyuminiehvikh-splaviv.html
6. Puzhailo, L. P., Siryi, O. V., Polyvoda, S. L. (2015). Pat. No. 108781 UA. Sposib rafinuvannia aliuminiievoho splavu u vakuumi. MPK C22B 21/00, C22B 9/04. No. a201310432. declareted: 27.08.2013; published: 10.06.2015, Bul. No. 11. Available at: https://uapatents.com/4-108781-sposib-rafinuvannya-alyuminiehvogo-splavu-u-vakuumi.html
7. Ostash, O. P., Polyvoda, S. L., Narivskyi, A. V., Chepil, R. V., Podhurska, V. Ya., Kulyk, V. V. (2020). Vplyv khimichnoho skladu na strukturu ta mekhanichni i koroziini vlastyvosti lytykh splaviv systemy Al-Mg-Sc. Fizyko-khimichna mekhanika materialiv, 56 (4), 122–127.
8. Gavras, A. G., Chenelle, B. F., Lados, D. A. (2010). Effects of microstructure on the fatigue crack growth behavior of light metals and design considerations. Matéria (Rio de Janeiro), 15 (2), 319–329. doi: https://doi.org/10.1590/s1517-70762010000200033
9. Avtokratova, E., Sitdikov, O., Kaibyshev, R., Watanabe, Y. (2008). Fatigue-Crack-Growth Behavior of Ultrafine-Grained Al-Mg-Sc Alloy Produced by ECAP. Materials Science Forum, 584-586, 821–826. doi: https://doi.org/10.4028/www.scientific.net/msf.584-586.821
10. Mann, V. Kh., Krokhin, A. Iu., Alabin, A. N., Khromov, A. P. (2019). Pat. No. 2 683 399 C1 RU. Splav na osnove aliuminiia. Opubl. 23.03.2019; Biul. No. 10.
11. Derkach, F. A. (1968). Khimiia, Lviv: Lvivsk. universytet, 311.
12. Ostash, O. P., Kostyk, E. M., Kudriashov, V. G., Andreiko, I. N., Skotnikov, I. A. (1990). Nizkotemperaturnaia tciklicheskaia treshchinostoikost vysokoprochnykh aliuminievykh splavov na stadiiakh zarozhdeniia i rosta treshchiny. Fiziko-khimicheskaia mekhanika materialov, 26 (3), 40–49.
13. Ostash, O. P., Labur, T. M., Holovatiuk, Yu. V., Vira, V. V., Koval, V. A., Shynkarenko, V. S., Yavorska, M. R. (2019). Konstruktsiina mitsnist zvarnykh ziednan termozmitsnenoho splavu systemy Al-Cu-Mg. Fizyko-khimichna mekhanika materialiv, 4, 81–87.
14. Ostash, O. P. (2006). Novi pidkhody v mekhanitsi vtomnoho ruinuvannia. Fizykokhimichna mekhanika materialiv, 26 (3), 13–25.
15. Ostash, O. P., Chepil, R. V., Titov, V. A., Polyvoda, S. L., Voron, M. M., Podhurska, V. Ya. (2021). Mitsnist i tsyklichna trishchynostiikist termodeformovanykh splaviv systemy Al-Mg-Sc. Fizyko-khimichna mekhanika materialiv, 57 (3), 118–125.
16. Zhemchuzhnikova, D., Mogucheva, A., Kaibyshev, R.; Weiland, H., Rollett, A., Cassada, W. (Eds.) (2012). Mechanical properties of Al-Mg-Sc-Zr alloys at cryogenic and ambient

temperatures. Proc. 13th Int. Conf. on Aluminium Alloys (ICAA13). The Minerals, Metals and Materials Society, 879–884. doi: https://doi.org/10.1002/9781118495292.ch131

17. Mogucheva, A., Babich, E., Kaibyshev, R.; Weiland, H., Rollett, A., Cassada, W. (Eds.) (2012). Microstructure and mechanical properties of an Al-Mg-Sc-Zr alloy subjected to extensive cold rolling. Proc. 13th Int. Conf. on Aluminium Alloys (ICAA13). The Minerals, Metals and Materials Society, 1773–1778. doi: https://doi.org/10.1007/978-3-319-48761-8_265
18. Ostash, O. P., Kostyk, E. M., Levina, I. N. (1988). Vliianie nizkoi temperatury na zarozhdenie i rost ustalostnykh treshchin v stali 08kp s razlichnym razmerom zerna. Fiziko-khimicheskaia mekhanika materialov, 24 (4), 63–71.
19. Ivasyshyn, A. D., Vasyliv, B. D. (2001). Vplyv rozmiriv i formy zrazkiv na diahramu shvydkostei rostu vtomnykh trishchyn. Fizyko-khimichna mekhanika materialiv, 37 (6), 119–120.
20. Holovatiuk, Yu. V., Pokliatskyi, A. H., Ostash, O. P., Labur, T. M. (2018). Pidvyshchennia konstruktsiinoi mitsnosti zvarnykh z'iednan lystiv zi splavu systemy Al-Cu-Mg. Fizyko-khimichna mekhanika materialiv, 54 (3), 112–119.
21. Nie, Z. R., Fu, I. B., Zon, I. X., Jin, T. N., Yang, I. I., Xu, G. F., et al.; Nie, I. E., Morton, A. J., Muddle, B. C. (Eds.) (2004). Advanced aluminium alloys containing rare-earth erbium. Proc. 9th Int. Conf. on Aluminium Alloys. Brisbane, 197–201.
22. He, L. Z., Li, X. H., Liu, X. T., Wang, X. J., Zhang, H. T., Cui, J. Z. (2010). Effects of homogenization on microstructures and properties of a new type Al-Mg-Mn-Zr-Ti-Er alloy. Materials Science and Engineering: A, 527 (29-30), 7510–7518. doi: https://doi.org/10.1016/j.msea.2010.08.077
23. la Torre, E. A.-D., Pérez-Bustamante, R., Camarillo-Cisneros, J., Gómez-Esparza, C. D., Medrano-Prieto, H. M., Martínez-Sánchez, R. (2013). Mechanical properties of the A356 aluminum alloy modified with La/Ce. Journal of Rare Earths, 31 (8), 811–816. doi: https://doi.org/10.1016/s1002-0721(12)60363-9
24. Zhang, X., Wang, Z. H., Zhou, Z. H., Xu, J. M., Zhong, Z. J., Yuan, H. L., Wang, G. W. (2015). Effects of Rare Earth on Microstructure and Mechanical Properties of Al-3.2Mg Alloy. Materials Science Forum, 817, 192–197. doi: https://doi.org/10.4028/www.scientific.net/msf.817.192
25. Pozdniakov, A. V., Yarasu, V., Barkov, R. Yu., Yakovtseva, O. A., Makhov, S. V., Napalkov, V. I. (2017). Microstructure and mechanical properties of novel Al-Mg-Mn-Zr-Sc-Er alloy. Materials Letters, 202, 116–119. doi: https://doi.org/10.1016/j.matlet.2017.05.053
26. Ibrokhimov, S. Zh. (2018). Struktura i svoistva splava AMg4, legirovannogo redkozemelnymi metallami (Sc, Y, La, Pr, Nd). Dushanbe.
27. Ostash, O. P., Polivoda, S. L., Chepil, R. V., Titov, V. A., Gogaev, K. O., Kulik, V. V. et al. (2021). Vpliv ridkisnozemelnikh metaliv na strukturu i vlastivosti litikh ta deformovanikh splaviv sistemi Al-Mg-Cr-Sc-Zr. Fiziko-khimichna mekhanika materialiv, 57 (6), 120–127.
28. Estrin, Y., Vinogradov, A. (2013). Extreme grain refinement by severe plastic deformation: A wealth of challenging science. Acta Materialia, 61 (3), 782–817. doi: https://doi.org/10.1016/j.actamat.2012.10.038

29. Zhemchuzhnikova, V. A. (2016). Vliianie deformatcii na strukturu i mekhanicheskie svoistva Al-Mg-Sc-Zr splava. Belgorod.
30. Ren, L., Gu, H., Wang, W., Wang, S., Li, C., Wang, Z., Zhai, Y., Ma, P. (2020). The Microstructure and Properties of an Al-Mg-0.3Sc Alloy Deposited by Wire Arc Additive Manufacturing. Metals, 10 (3), 320. doi: https://doi.org/10.3390/met10030320
31. Harada, Y., Dunand, D. C. (2009). Microstructure of Al_3Sc with ternary rare-earth additions. Intermetallics, 17 (1-2), 17–24. doi: https://doi.org/10.1016/j.intermet.2008.09.002
32. Fang, H. C., Shang, P. J., Huang, L. P., Chen, K. H., Liu, G., Xiong, X. (2012). Precipitates and precipitation behavior in Al-Zr-Yb-Cr alloys. Materials Letters, 75, 192–195. doi: https://doi.org/10.1016/j.matlet.2012.02.013
33. Iakiviuk, O. V. (2018). Razrabotka tekhnologii polucheniia dlinnomernykh deformirovannykh polufabrikatov iz splavov sistemy Al-Mg, legirovannykh skandiem, i issledovanie ikh svoistv. Krasnoiarsk.
34. Bethencourt, M., Botana, F. J., Calvino, J. J., Marcos, M., Rodríguez-Chacón, M. A. (1998). Lanthanide compounds as environmentally-friendly corrosion inhibitors of aluminium alloys: a review. Corrosion Science, 40 (11), 1803–1819. doi: https://doi.org/10.1016/s0010-938x(98)00077-8
35. Cavaliere, P. (2009). Fatigue properties and crack behavior of ultra-fine and nanocrystalline pure metals. International Journal of Fatigue, 31 (10), 1476–1489. doi: https://doi.org/10.1016/j.ijfatigue.2009.05.004
36. Titov, A. V., Balushok, K. B., Ostash, O. P., Titov, V. A., Korieva, V. O., Polyvoda, S. L., Chepil, R. V. (2022). Presuvannia napivfabrykativ zi splaviv systemy Al-Mg-Sc v izotermichnykh umovakh. Fizyko-khimichna mekhanika materialiv, 58 (5), 120–127.
37. Design Environment for FORMing. Available at: https://www.deform.com/products/deform-3d/
38. Kolmohorov, V. L. (1970). Napriazhenyia, deformatsyy, razrushenye. Moscow: Metallurhyia, 229.
39. Bohatov, A. A., Myzhyrytskyi, O. Y., Smyrnov, S. V. (1984). Resurs plastychnosty metallov pry obrabotke davlenyem. Moscow: Metallurhyia, 144.
40. Mykhalevych, V. M., Dobraniuk, Yu. V., Kraievskyi, V. O. (2018). Porivnialne doslidzhennia modelei hranychnykh plastychnykh deformatsii. Visnyk mashynobuduvannia ta transportu, 2 (8), 56–64.
41. Shao, Y., Peng, W., Cao, F., Oleksandr, M., Titov, V. (2022). Effect of process parameters on AA6061/Q345 bimetal composite for hot stamping. Proceedings of the Institution of Mechanical Engineers, Part E: Journal of Process Mechanical Engineering, 236 (6), 2515–2525. doi: https://doi.org/10.1177/09544089221096204
42. Yu, Z., Peng, W., Zhang, X., Oleksandr, M., Titov, V. (2022). Evolution of microstructure of aluminum alloy hollow shaft in cross wedge rolling without mandrel. Journal of Central South University, 29 (3), 807–820. doi: https://doi.org/10.1007/s11771-022-4950-8